Improved correspondence of fMRI visual field localizer data after macroanatomical alignment

Running Title: Visual field localizer & CBA

Qubad M.[1], Barnes-Scheufler C.V.[1], Schaum M.[2], Raspor E.[1], Rösler L.[1,3], Peters B.[4,5], Goebel R.[3,6], Reif A.[1], Bittner R.A.[1,7]*

[1] Department of Psychiatry, Psychosomatic Medicine and Psychotherapy and Brain Imaging Center, University Hospital, Goethe University, Frankfurt, Germany,

[2] Leibniz Institute for Resilience Research, Mainz, Germany

[3] Netherlands Institute for Neuroscience, Amsterdam, The Netherlands

[4] Institute of Medical Psychology, University Hospital, Goethe University, Frankfurt, Germany,

[5] Zuckerman Mind Brain Behavior Institute, Columbia University, New York, NY, USA

[6] Department of Cognitive Neuroscience, Faculty of Psychology and Neuroscience, Maastricht University, Maastricht, The Netherlands

[7] Ernst Strüngmann Institute for Neuroscience (ESI) in Cooperation with Max Planck Society, Frankfurt am Main, Germany

[*]Corresponding author. Department of Psychiatry, Psychosomatic Medicine and Psychotherapy, University Hospital Frankfurt, Goethe University, Heinrich-Hoffmann-Str. 10, D-60528 Frankfurt am Main, Germany.
Phone: +49 69 6301 84713. Fax: +49 69 6301 81775.
Email: bittner@med.uni-frankfurt.de

Total number of words in abstract: 227

Total number of words in text: 5501

ORCID IDs

M.Q.: orcid.org/0000-0002-9291-5739

C.V.B.-S.: orcid.org/0000-0002-4730-1981

M.S.: orcid.org/0000-0002-6589-4530

E.R.: orcid.org/0000-0003-4418-7084

L.R.: orcid.org/0000-0003-1046-1073

B.P.: orcid.org/0000-0002-0948-8976

R.G.: orcid.org/0000-0003-1780-2467

A.R.: orcid.org/0000-0002-0992-634X

R.A.B.: orcid.org/0000-0003-2021-0358

ACKNOWLEDGEMENTS

The authors are most grateful to Deliah Macht, Christina Raab and Leonie Winkler-Lauble for help with data acquisition. C.V Barnes-Scheufler was supported by a “main doctus” scholarship from The Polytechnic Foundation of Frankfurt am Main. E. Raspor was supported by a Research Grant for Doctoral Programmes in Germany from The German Academic Exchange Service (DAAD).

ABSTRACT

The study of the visual system and its role for human cognition in health and disease with fMRI often requires the use of localizer paradigms to define anatomical regions of interest (ROIs). However, the considerable degree of interindividual variability of the cerebral cortex represents an important confound, especially when analyzing visual localizer data on the group level. Cortex-based alignment (CBA) techniques lead to a reliable reduction of interindividual anatomical variability. Yet, the potential benefits of CBA has not been investigated for visual field localizer paradigms used to map specific parts of the visual field within retinotopically organized early visual areas. We evaluated CBA for an attention-enhanced visual field localizer mapping a homologous part of each visual quadrant in a cohort of 50 participants. After CBA, group ROIs showed markedly increased spatial consistency. CBA also led to an increase in the probability of activation overlap of up to forty percent. Furthermore, the size of group ROIs for the lower visual hemifield was larger than for the upper visual hemifield after CBA. This asymmetry, which mirrors previous findings from electrophysiological and fMRI studies, was not detectable before CBA. Our results confirm and extend the utility of CBA for the study of the visual system particularly in the context of group analyses. This method should be particularly important for the study of neuropsychiatric disorders with abnormally increased interindividual anatomical variability.

KEYWORDS

Human visual cortex, fMRI, visual-field localizer, cortex-based alignment

76

INTRODUCTION

The visual system includes a multitude of topographical representations of varying resolution across increasingly specialized visual areas (Wandell, Dumoulin, & Brewer, 2007). Functional magnetic resonance imaging (fMRI) offers a variety of methods either to map these topographical representations in full, or to localize specific visual areas or retinotopic positions within their topography. These approaches are essential not only for the fine-grained study of fundamental properties of the visual system (Wandell et al., 2007), but also for investigating the role of these areas for higher-order cognitive processes such as visual attention and working memory (Bergmann, Genç, Kohler, Singer, & Pearson, 2014; Corbetta & Shulman, 2002; Das, Bennett, & Dutton, 2007; de Haan, Bither, Brauer, & Karnath, 2015; Goodale & Milner, 2006; Ungerleider, 1982). This also extends to translational studies of visual dysfunction and its cognitive consequences in neuropsychiatric disorders (Lee et al., 2019; Silverstein et al., 2009).

Methods for fMRI-based visual mapping, i.e. techniques to define regions of interest (ROIs) in the visual system based on specific functional properties, fall in in three broad categories: retinotopic mapping, visual field localizer and functional localizer paradigms. Retinotopic mapping and the more advanced population receptive field mapping allow the complete delineation of early visual areas (Dumoulin & Wandell, 2008; Sereno et al., 1995; Wandell et al., 2007). Conversely, visual field localizer paradigms can map a circumscribed region within a retinotopically organized visual area (Harrison & Tong, 2009; Peters, Kaiser, Rahm, & Bledowski, 2015). Finally, functional localizers can detect higher-order visual areas such as the fusiform face area (Yenari, Xu, Tang, Qiao, & Giffard), parahippocampal place area (Sereno et al.), extrastriate body area (EBA), lateral occipital complex (LOC) etc., which are clustered and show specialization for the processing of specific categories of complex visual information (Downing, Chan, Peelen, Dodds, & Kanwisher, 2006; Kanwisher, McDermott, & Chun, 1997; Wandell et al., 2007). In most fMRI studies, high interindividual anatomical variability of cortical areas in terms of both size and location constitutes an important challenge (Brett, Johnsrude, & Owen, 2002; Desai, Liebenthal, Possing, Waldron, & Binder,

2005; Dougherty et al., 2003; Fischl, Sereno, & Dale, 1999; Frost & Goebel, 2012, 2013; Steinmetz, Fürst, & Freund, 1990; Van Essen et al., 2001; Zilles et al., 1997). For instance, it has been shown, that primary visual cortex (V1) can differ in size by about 2-fold between individuals (Dougherty et al., 2003). Furthermore, anatomical variability in terms of location has been shown to be particularly pronounced in extrastriate visual areas (Bridge, 2011). This crucial confound reduces the power to reliably map visual areas at the group level. One way to mitigate this problem for the visual system is to pool single-subject ROIs, while simultaneously using the overall group-based probability for that ROI at each point in a Cartesian coordinate system as a constraint (Fedorenko, Hsieh, Nieto-Castañón, Whitfield-Gabrieli, & Kanwisher, 2010; Julian, Fedorenko, Webster, & Kanwisher, 2012; Nieto-Castañón & Fedorenko, 2012). While such a single-subject-based analysis improves sensitivity and functional resolution compared to a standard group-based approach, it does not actually reduce macroanatomical variability. Additionally, studying the interplay between visual areas and other cortical areas more directly involved in higher-order cognitive processes might preclude a single-subject based strategy. This applies in particular to functional connectomic approaches such as small-world networks, which compute interactions between brain regions at the whole-brain level (Tost, Bilek, & Meyer-Lindenberg, 2012).

Cortex-based alignment (CBA) methods have been proposed as an alternative approach (Julian et al., 2012). CBA uses a geodesic coordinate system, which allows for a two-dimensional representation of the cerebral cortex, which respects the cortical topography to much larger degree than a traditional Cartesian coordinate system (Anticevic et al., 2008; Frost & Goebel, 2012; Julian et al., 2012). This representation allows the use of individual cortical folding patterns for a fully data-driven macroanatomical alignment. Compared to traditional nonlinear volume-based alignment (NVA) procedures (Evans et al., 1993; Talairach, 1988), CBA considerably improves anatomical correspondence of cortical structures (Anticevic et al., 2008; Fischl, Sereno, & Dale, 1999; Fischl, Sereno, Tootell, & Dale, 1999; Pantazis et al., 2010; Van Essen & Drury, 1997).

Several studies have compared the impact of NVA and CBA methods on specific visual mapping techniques. For retinotopic mapping an improvement of functional overlap in both V1 and V2 after CBA has been demonstrated (Fischl, Sereno, Tootell, et al., 1999; Hinds et al., 2008). Furthermore, for functional localizer data CBA substantially increases the overlap of object processing areas LOC, FFA and PPA across subjects (Frost & Goebel, 2012; Huang, Chen, Jiang, Zhen, & Liu, 2019; Rosenke, van Hoof, van den Hurk, Grill-Spector, & Goebel, 2020; Weiner et al., 2018). Conversely, the effects of CBA on visual field localizer paradigms mapping specific retinotopic positions have not been studied. Thus, the utility of CBA has been demonstrated for two of the three main categories of visual mapping methods, i.e. those methods, which map whole areas, either defined by cytoarchitectonic (e.g. V1) or functional (e.g. FFA) properties. Conversely, it remains unclear, to which degree CBA can improve the alignment of ROIs mapped by visual field localizer paradigms.

Such paradigms are required for the detailed study of the local processing of simple visual stimuli in early visual areas (Di Russo, Martínez, & Hillyard, 2003; Di Russo, Martínez, Sereno, Pitzalis, & Hillyard, 2002; Harrison & Tong, 2009; Peters et al., 2015; Shigihara, Hoshi, & Zeki, 2016). Flashing chequerboards covering the exact area of interest within the visual field are primarily used for this purpose. Chequerboards lead to a particularly strong BOLD-signal increase in early visual areas (V1-V3) (Kraft et al., 2005). To maximize the fidelity of the resulting localizer maps, visual field localizer paradigms typically utilize the fact that attentional modulation induced by task demands significantly enhances response reliability across visual areas. This can be accomplished by adding a simple target detection task (Bressler & Silver, 2010).

We used such an attention-enhanced visual field localizer paradigm to map a circumscribed location in each visual quadrant across early visual areas in order to define ROIs to be used for the study of higher cognitive processes. We chose a CBA method using a dynamic group average as the target brain (Frost & Goebel, 2012). Thus, we eliminated the possible confound of a static CBA target based on an individual brain, whose cortical folding pattern might by chance deviate considerably from the group average.

Our primary goal was to examine the effects of CBA for a visual field localizer paradigm. More specifically, we aimed to determine, whether CBA can improve the reliability of mapping subregions within retinotopically organized visual areas delineated by such a paradigm at the group level. Based on previous findings for other localizer paradigm classes and the relatively good structural-functional correspondence in posterior occipital cortex, we expected to observe a benefit of CBA when aligning subregions within early visual cortex. Additionally, we compared the two main methods for the definition of single subject ROIs: the use of peak vertices, i.e. single vertices showing the strongest level of activation in a certain brain region, and the delineation of a larger ROI, which includes all vertices above a prespecified threshold, which is kept constant across brain regions (Tong et al., 2016). Our goal was to compare these two approaches and to assess changes in spatial correspondence after CBA at the single subject level. Mirroring our hypotheses for the group analyses, we expected to observe an improved correspondence of single-subject peak-vertex ROIs after CBA.

Interestingly, several studies have shown differential response properties such as receptive field size for homologous early visual areas by visual quadrant or hemifield. For instance, improved behavioral performance and higher BOLD-signal amplitudes were observed in the lower visual hemifield (Anderson, Cameron, & Levine, 2014; Liu, Heeger, & Carrasco, 2006; O'Connell et al., 2016; Rubin, Nakayama, & Shapley, 1996). We were therefore also interested, whether we could observe differences between upper and lower visual hemifields in our group analysis after CBA. Overall, the aim of the study was to close an important gap in the evaluation of CBA for the study of the visual system. Since visual field localizers are crucial for investigating the contribution of the visual system to higher-order cognitive processes, our results should have implications for the study of visual cognition in both for basic and translational research.

METHODS AND MATERIALS

Participants:

All participants gave their written consent to participate in the study. The ethical review board of the Faculty of Medicine at Goethe University granted ethic approval. We recruited 51 healthy volunteers (male: female = 23: 28) with age ranging between 18-43 years (mean = 24). All participants were non-smokers, had no history of neurological or psychiatric illness and reported normal or corrected-to-normal visual acuity. One participant was left-handed as assessed by the German version of the Edinburgh Handedness Inventory (Oldfield, 1971).

Stimuli and task:

Subjects performed a visual field localizer paradigm (Figure 1) implemented using Presentation® (Neurobehavioral Systems, Version 18.0) as part of a larger study investigating the role of visual areas for higher cognitive functions. The task consisted of a series of flickering black-and-white-colored round shaped chequerboard stimuli (flicker frequency = 7.5 Hz). Chequerboard stimuli appeared for 2000 ms randomly at one of four different locations (non-target trial). Each location mapped a homologous position in one of the four visual quadrants. Our paradigm featured a simple target-detection task. During thirty-six trials, the two centrally located squares of the chequerboard changed their color to yellow for 133 ms (target trial). Participants were instructed to press a response box button with their left thumb as quickly as possible if they detected a target. The task consisted of a total of 144 trials (36 target trials, 108 standard trials). Thus, target probability was 25 %. The regular inter-stimulus interval was 0 ms. However, once every 10 to 14 trials the inter-stimulus interval increased to 2000 ms. Throughout the task a black, x-shaped fixation cross was displayed at the center of the screen. Participants were instructed to continuously fixate on the fixation cross. Before the first trial, only the fixation cross was displayed for 10 seconds. After the last trial, only the fixation cross was displayed for 20 seconds. The total duration of the paradigm was 340 seconds. For the purpose of our analyses we defined a

total of four conditions, one for each of the four stimulus locations. Each participant practiced the task prior to the measurement.

Acquisition of fMRI data:

We acquired functional MRI data on a Siemens 3T MAGNETOM Trio scanner at the Goethe University Brain Imaging Centre using a gradient-echo EPI sequence (32 axial slices, TR = 2000 ms, TE = 30 ms, FA = 90°, FoV = 192 x 192 mm2, voxel size = 3 x 3 x 3 mm3, gap = 1 mm). Slices were positioned parallel to the anterior- and posterior commissure. Functional images were acquired in a single run comprising the acquisition of 170 volumes. Stimulus presentation was constantly synchronized with the fMRI sequence. Head motion was minimized with pillows. The task was projected by a beamer onto a mirror attached on the head coil. Anatomical MRI data for cortex reconstruction and co-registration with functional MRI data was acquired with a high-resolution T1-weighted 3D volume using a Magnetization-Prepared Rapid Gradient-Echo (MP-RAGE) sequence.

Functional image pre-processing:

MRI data were pre-processed and analyzed using Brain Voyager 20.6 (Goebel, Esposito, & Formisano, 2006), the NeuroElf toolbox (www.neuroelf.net) and custom software written in Matlab. Structural data pre-processing included brain extraction, inhomogeneity correction and transformation into Talairach coordinate space. Initial volume-based pre-processing of functional MRI data included slice scan time correction and motion correction.
At this stage, one subject had to be excluded due to excessive intra-scan motion.
After co-registration to the anatomical scans with a boundary-based registration algorithm (Greve & Fischl, 2009), the functional data were transformed into Talairach coordinate space.
Based on the segmentation of the structural scans along the white–grey matter boundary (Kriegeskorte & Goebel, 2001), cortical hemispheres were first reconstructed into folded, topologically correct mesh representations, which were tessellated to produce surface

reconstructions. These were subsequently morphed into spherical representations. We then applied a high-resolution, multiscale cortex-based alignment procedure, which reliably aligns corresponding gyri and sulci across subjects (Bittner et al., 2017; Goebel et al., 2006). This CBA approach consists of an initial rigid and a subsequent non-rigid alignment step (Frost & Goebel, 2012). During the initial step, we aligned the cortical folding pattern of each sphere rigidly to the cortical folding pattern of a target sphere by global rotation. We used the resulting rotation parameters with the highest overlap between the curvature of a subject's sphere and the target sphere as a starting point for the subsequent non-rigid CBA. In this step, we aligned each cortical folding pattern to a dynamically updated group average through iterative morphing following a coarse-to-fine matching strategy. During the initial rigid alignment step, we aimed to avoid the possible confounding effects of a suboptimal selection of an individual target brain, whose folding pattern might deviate considerably from the cohort average. To this end, we conducted a preliminary non-rigid CBA procedure, which included the brains of all 50 participants. The results of this preliminary non-rigid CBA procedure were only used to generate unbiased average brains to be used as targets for the initial rigid alignment step.

The volumetric functional data were then sampled on the cortical surface incorporating data from −1 to +3 mm along vertex normals. Based on the vertex-to-vertex referencing from the folded, topologically correct meshes to the aligned spherical representations, we mapped the functional data into a common spherical coordinate system. Finally, surface-based pre-processing of functional MRI data included spatial smoothing using a nearest neighbor interpolation (1 iteration, approximating a 2D Gaussian smoothing kernel with a FWHM of 1 mm), temporal high-pass filtering (high-pass 0.00903 Hz) and linear trend removal. Spatial smoothing in surface space is clearly superior to spatial smoothing in volume space (Brodoehl, Gaser, Dahnke, Witte, & Klingner, 2020). However, we still opted for minimal spatial smoothing to minimize the loss of accuracy for our visual field localizer.

271 Cortex-based group fMRI analysis:

272 We performed multi-subject statistical analyses using multiple linear regression of the BOLD
273 signal. The presentation of each chequerboard stimulus sequence at a single location, was
274 modelled by an ideal box-car function, which covered the volume of each trial, convolved
275 with a synthetic two-gamma function. These predictors were used to build the design matrix
276 of the experiment. Individual statistical maps were generated by associating each voxel with
277 the F-value corresponding to the specific set of predictors and calculated on the basis of the
278 least mean squares solution of the general linear model. We created anatomical masks that
279 only included cortical vertices in our analysis. These masks excluded those subcortical
280 structures, i.e. parts of thalamus and the basal ganglia, which mapped onto the midline of our
281 surface reconstructions.

282

283 Group analysis of visual quadrants before and after CBA:

284 We performed analyses focusing on the mapping of the four visual quadrants at the group
285 level and compared these with results at single subject level. To define the group level ROI
286 for each visual quadrant, we computed separate weighted contrasts for each quadrant
287 against the other three quadrants. We assigned a weight of three to the position of interest,
288 e.g. $(\beta^{Quad1} \times 3) / (\beta^{Quad2} + \beta^{Quad3} + \beta^{Quad4})$ ($p < 0.5$, Bonferroni corrected). For each resulting
289 group level ROI, we extracted average time courses (incl. standard errors of the mean =
290 SEM) for all four conditions. We conducted this analysis both before and after CBA.

291

292 Probability maps before and after CBA:

293 To quantify and visualize variability of functional activation and possible changes due to
294 macroanatomical alignment, the use of probability maps has been proposed. Probability
295 maps are specifically useful to quantify inconsistency i.e. the disparity between individuals
296 regarding the location of a particular (visual) area. To quantify the spatial consistency of
297 activation patterns before and after CBA, we generated probability maps for each visual
298 quadrant (Wang, Mruczek, Arcaro, & Kastner, 2015; Yamamoto et al., 2012). These maps

represent the relative number of subjects showing significant task activity in our single-subject analysis. Probability maps for early visual areas before and after CBA were created based on the previously generated single subject t-maps, with a threshold of a minimum of ten percent probability. To quantify the change in spatial consistency of activation patterns as a result of CBA, we created probability difference maps for each position (post-CBA minus pre-CBA). This allowed us to determine both increases and decreases of spatial consistency due to CBA.

Single-subject ROIs of visual quadrants before and after CBA including peak vertex mapping:

For analyses at single-subject level, we first defined ROIs for each subject independently using the same weighted contrasts employed in the group analysis. We applied a more lenient statistical threshold ($p < 0.05$ uncorrected). For each resulting single-subject ROI we extracted average time courses for all four conditions. We then averaged these time courses across all subjects. Thus, we generated group level average time courses reflecting each subject's region of maximum activation. We conducted this analysis both before and after CBA. Additionally, we determined the peak vertex for each subject's four visual quadrant ROIs, i.e. the vertex with the highest t-value. We then defined extended single-subject peak vertex ROIs, which also included the six vertices adjacent to the peak vertex (Tong et al., 2016). For each resulting single-subject peak vertex ROI we extracted average time courses (incl. SEM) for all four conditions. We then averaged these timecourses across all subjects. We conducted this analysis both before and after CBA.

Peak vertex distribution maps:

We mapped all peak vertices per visual quadrant before and after CBA and computed the vertex-wise number of peak vertices to estimate the degree of overlap between subjects.

RESULTS

Impact of CBA on spatial consistency of ROIs (group level)

Group-level mapping of the four visual quadrants revealed considerable differences before and after CBA. For the right lower visual quadrant, our analysis before CBA yielded a large cluster in the left upper occipital cortex, also encompassing posterior parts of temporal cortex, which decreased considerably in size after CBA and was much more circumscribed. Conversely, for the other three visual quadrants, our analysis before CBA yielded clusters in the corresponding parts of the occipital pole, which increased in size after CBA without a notable change of their center of gravity (Figure 2, Table 1). Overall, after CBA group ROIs showed markedly greater spatial consistency and vertical symmetry. Additionally, after CBA, ROIs for the lower visual hemifield were considerably larger in size than ROIs for the upper visual hemifield. Before and after CBA, average time courses showed clear position selectivity which increased after CBA (Figure 2).

Probability maps (group level)

Before CBA, probability maps showed a relatively wide spread of functional activation around the core region of interest defined in our previous group analysis (Figure 3). The maximum probability of overlap of around 50 % was consistently located at the center of each ROI. After CBA, probability maps showed a noticeable decrease in the spread of functional activation around the core region of interest with a corresponding increase in the maximum probability of overlap. Consequently, probability difference maps (Figure 4) showed an increase in the probability of overlap of up to 40 % around the core region of interest and a corresponding peripheral decrease in the probability of overlap of up to 40 %.

Comparison of full ROIs and extended peak-vertex ROIs (single-subject level)

The comparison of time courses averaged over all full single subject ROIs with time courses averaged over all single subject extended peak-vertex ROIs showed consistently larger BOLD signal amplitudes for extended peak-vertex ROIs (Figure 5). There was no difference

in BOLD signal amplitude before and after CBA for both types of ROI. Before and after CBA, all ROIs showed comparable clear position selectivity.

The rate of success for finding a ROI for each subject was as follows: upper right visual quadrant 46 out of 50 subjects, upper left visual quadrant 50 out of 50 subjects, lower left visual quadrant 48 out of 50 subjects, lower right visual quadrant 50 out of 50 subjects.

Impact of CBA on spatial variability of peak vertex distribution (single-subject level)

As with the probability maps at the group level, peak vertex distribution maps at the single-subject level (Figure 6) showed less spatial variability after CBA with an increased probability of overlap. Both before and after CBA, the spread of peak vertices was larger for the lower visual quadrants.

DISCUSSION

The aim of our study was to evaluate the utility of CBA for a visual field localizer paradigm used to map a circumscribed region within retinotopically organized visual areas. Our paradigm mapped homologous regions in each visual quadrant reliably across early visual areas. As expected, CBA led to a marked reduction in macroanatomical variability. On the functional level, CBA had a number of beneficial effects.

CBA improved the results of the group ROI analysis for all visual quadrants (Figure 2). This was reflected in both the spatial consistency of the resulting group ROIs and in the signal-to-noise ratio exemplified by the difference between the BOLD signal amplitude for the stimulated location compared to the other locations. Probability difference maps showed an increase in the probability of overlap of up to forty percent in the central region of interest, which resulted in considerably more focused activation patterns. However, the opposite effect was observed in more peripheral vertices (Figure 4). The latter effect is most likely not attributable to a decrease of spatial overlap in the periphery of early visual areas. Rather it demonstrates that CBA consistently reduces spurious spread-out activation resulting from

poor macroanatomical correspondence after NVA. This observation suggests that NVA-based group analyses generally overestimate the extent of visual areas.

Together these findings indicate that CBA substantially increases statistical power when studying early visual areas at the group level. Naturally, this effect of CBA also extends to studies with a more global focus, such as connectivity analyses (Brodoehl et al., 2020; Bullmore & Sporns, 2009).

Regarding the comparison between full single-subject ROIs and extended peak-vertex single-subject ROIs, we made the following observations. As expected, BOLD signal amplitudes for single subject ROIs were not affected by CBA (Figure 5). Conversely, the variability of these ROIs as signified by the peak vertex location decreased after CBA (Figure 6). This underscores that the reduction of functional inter-subject variability due to CBA is the main reason for our improved results at the group level. Furthermore, BOLD signal amplitudes for the full single-subject ROIs were consistently lower compared to our extended single-subject peak vertex ROIs (Figure 5). This is well in line with previous findings of larger effect sizes in volume space for strategies using peak-voxels with or without including directly neighboring voxels to define ROIs (Tong et al., 2016).

Before CBA we observed the strongest group effects, i.e. the largest group ROIs, for the left lower and right upper visual quadrant, an effect that clearly did not persist after CBA (Figure 2). Notably, several studies using volume-based fMRI and magnetoencephalographic (Hahn et al.) analyses reported lateralized effects on neurophysiological parameters in early visual areas (H. Chen, Yao, & Liu, 2004; Loughnane, Shanley, Lalor, & O'Connell, 2015). Our observation raises the question, whether these findings could at least partly be explained by lateralized differences in macro-anatomical variability rather than true functional differences. Conversely, our CBA-aided group analysis allowed us to compare the response properties of each visual quadrant in a more unbiased way. We observed larger group ROIs for the lower visual hemifield. In a CBA-based probabilistic atlas of the visual system, which included all regions that could be defined in more than 50% of subjects, probabilistic ROIs for dorsal V1 and V2 were also noticeably larger than probability maps for ventral V1 and V2, whereas this

effect was less clear for V3 (Rosenke et al., 2020). These results are in line with our own findings and could be attributable to higher residual anatomical variability after CBA in ventral occipital cortex representing the upper visual hemifield. Alternatively, they could be due to true differences in response properties such as receptive field size or overall area size. The latter interpretation is supported by studies showing functional differences between upper and lower visual hemifields already at the retinal level in the form of differences in receptor densities. Cone density was higher in the superior parts of the retina which processes information from lower visual fields. Conversely, higher rod density was observed in the inferior parts (Curcio & Allen, 1990; Eickhoff, Rottschy, Kujovic, Palomero-Gallagher, & Zilles, 2008). Moreover, Eickhoff et al. observed dorso-ventral asymmetries in receptor densities in V2 and V3 (Eickhoff et al., 2008). They found a higher density of GABA-A, benzodiazepine- as well as muscarinic M3-receptors in ventral parts of V2 and V3. Furthermore, there is evidence for fundamental differences in receptive field shape from a pRF mapping study. Estimating both the aspect ratios and the size of the mapped areas, a more elliptical receptive field shape was observed for the upper visual hemifield represented by ventral parts of the visual cortex being compared to the lower visual hemifield represented by dorsal parts of the visual cortex (Silson, Reynolds, Kravitz, & Baker, 2018). Additionally, there is evidence for a behavioral advantage in the lower visual hemifield for shape discrimination as well as higher BOLD-signal changes and peak amplitudes of MEG/EEG responses (Anderson et al., 2014; Hagler, 2014; O'Connell et al., 2016; Rubin et al., 1996; Schmidtmann, Logan, Kennedy, Gordon, & Loffler, 2015). Together, these findings demonstrate clear differences in the functional architecture of early visual areas representing the upper and lower visual hemifield. This has been attributed to the fact that the lower visual hemifield represented by dorsal parts of the occipital lobe is more closely linked to the dorsal visual pathway, while the upper visual hemifield represented by ventral parts of the occipital lobe is more closely linked to the ventral visual pathway (Thomas & Elias, 2011; Zito, Cazzoli, Müri, Mosimann, & Nef, 2016). Furthermore, there is evidence for fundamental differences in receptive field shape from a pRF mapping study. For the upper visual hemifield

represented by ventral parts of the visual cortex an increased size and more elliptical shape of receptive fields was observed compared to the lower visual hemifield represented by dorsal parts of the visual cortex (Silson, Reynolds, Kravitz, & Baker, 2018). This implies, that the lower visual field is more specialized for the precise localization and representation of space. Our observation of larger ROIs in the lower visual hemifield is in line with these findings. Thus, our results imply that CBA is a useful tool to extend the study of functional and behavioral asymmetries in early visual areas to the group level.

One important limitation of the current study is the lack of a complementary retinotopic mapping data set due to time constraints. This data would have allowed us to delineate the boundaries of early visual areas and pinpoint the exact visual area containing each individual single-subject ROI. Retinotopic mapping studies indicate that peak activation of single subjects assessed by visual localizers are not consistently located in the same visual area. Most localizer tasks show peak activation not in V1 but rather in V2 or V3 (Peters et al., 2015). It is therefore very likely that our single-subject peak activation did not consistently belong to the same visual cortical area. With the current data set we cannot determine how precisely individual visual areas were aligned with CBA, and whether individual levels of the visual cortical hierarchy were differentially affected.

However, the position of our group regions of interest, which bordered the calcarine sulcus and spanned the occipital pole, indicate that they mainly comprised V2 and V3. Similarly, after CBA a comparable increase in the probability of overlap was observed in the same part of occipital cortex. While this is at least suggestive of a relatively consistent benefit of CBA across visual areas, more fine-grained studies including retinotopic mapping are required to definitively address this question.

Furthermore, we did not use eye tracking to insure sufficient fixation. We also did not include an additional central attentional control task on the fixation cross, which would have further encouraged continuous fixation. This was done deliberately in order to keep the difficulty level adequate for psychiatric patient populations, but it might explain our failure to find reliable activation in early visual areas in a fraction of our subjects.

Our study also has implications beyond mapping the visual system in healthy populations. First, cortical processing in visual areas can to some degree be characterized more adequately by its task-specificity, rather than sensory-specificity (Amedi et al., 2007; Bedny, Pascual-Leone, Dodell-Feder, Fedorenko, & Saxe, 2011; Ptito, Matteau, Gjedde, & Kupers, 2009; Reich, Szwed, Cohen, & Amedi, 2011; Renier et al., 2005; Striem-Amit, Cohen, Dehaene, & Amedi, 2012). For instance, in blind people primary visual cortex can be adapted to map spatial locations of sound. It would be interesting to see, whether studying the retinotopic representation of spatial sound at the group level might also benefit from CBA (Norman & Thaler, 2019). Second, visual processing deficits are a prominent feature of neurodevelopmental psychiatric disorders such as ADHD, schizophrenia and autism spectrum disorders (Bakroon & Lakshminarayanan, 2016; Butler et al., 2001; Butler, Silverstein, & Dakin, 2008; C. Y. Chen et al., 2002; Hale et al., 2014; Lee et al., 2019; Sanz-Cervera, Pastor-Cerezuela, González-Sala, Tárraga-Mínguez, & Fernández-Andrés, 2017; Seymour, Rippon, Gooding-Williams, Schoffelen, & Kessler, 2019; Shimizu, Bueno, & Miranda, 2014; Silverstein et al., 2009). These deficits can also perturb crucial higher order cognitive processes including working memory, which underscores the relevance of visual dysfunction for pro-cognitive interventions (Bittner et al., 2015; Butler, Thompson, Seitz, Deveau, & Silverstein, 2017; Haenschel et al., 2007). Furthermore, perceptual processes are an explicit part of the Research Domain Criteria project, which aims to identify constructs of transdiagnostic relevance in order to establish a psychiatric nosology based on cognitive dimensions and the underlying brain networks (Cuthbert, 2014; Insel, 2014). Thus, the current localizer paradigm will be useful to investigate local impairments of visual information processing as well as disturbances in the interplay between early visual areas and brain networks supporting higher-order cognitive processes. In this context, an efficient mapping of the visual system capturing other aspects of the functional organization of the visual system such as retinotopy will be essential. This approach would benefit from a comprehensive visual mapping battery combining different localizer techniques. Here, CBA will be particularly relevant to reduce the confounding effects of increased macroanatomical

493 variability in disorders such as schizophrenia in order to detect true group differences and
494 true functional variability (Anticevic et al., 2008; Manoach, 2003). On the other hand, CBA
495 should also be crucial for investigating the neurodevelopmental underpinnings of increased
496 macroanatomical variability itself. To this end the inclusion of probabilistic atlases containing
497 information about gene expression profiles (French & Paus, 2015) as well as cyto- and
498 receptor archectonics (Gulban et al., 2020; Hawrylycz et al., 2012) will be valuable.
499 Our CBA approach relied solely on cortical curvature information to reduce macroanatomical
500 variability. The advantage of this method is its feasibility for the vast majority of fMRI data
501 sets, since it only requires a structural brain scan of sufficient quality. Among comparable
502 methods it is the most data driven and objective approach. However, the achievable degree
503 of reduction of macroanatomical variability is limited by the variable and imperfect correlation
504 between brain structure and brain function (Fischl, Sereno, Tootell, et al., 1999; Van Essen &
505 Drury, 1997). Therefore, more advanced methods additionally utilize orthogonal functional
506 data to further reduce anatomical variability. This includes the use of activation patterns or
507 functional connectivity patterns to improve macroanatomical alignment across the whole
508 brain (Conroy, Singer, Guntupalli, Ramadge, & Haxby, 2013; Frost & Goebel, 2013; Sabuncu
509 et al., 2009). Furthermore, a more complex approach has been proposed, which aligns
510 cortical data using ‘areal features’ more closely tied to cortical areas than cortical folding
511 patterns, including maps of relative myelin content and functional resting state networks
512 (Glasser et al., 2016). These methods have shown to provide a relevant additional reduction
513 of macroanatomical variability for a variety of paradigms including visual functional localizers.
514 Future studies should also evaluate these methods for retinotopic mapping and visual field
515 localizers. Moreover, it has been demonstrated for early auditory areas, that the additional
516 use of a probabilistic atlas of cytoarchitectonically defined areas further improves standard
517 CBA results (Tomasello, Wennekers, Garagnani, & Pulvermüller, 2019). Such an approach
518 would easily be feasible for the visual system.
519 To summarize, we demonstrated the clear superiority of CBA compared to NVA for the
520 analysis of visual field localizer data on the group level indicated by a forty percent increase

of overlap of ROIs. Our findings extend previous studies examining other major categories of visual mapping techniques. They underscore the comparable loss of information and statistical power incurred by the use of NVA methods in the majority of fMRI studies. Therefore, CBA and other comparable methods should be seriously considered as a standard procedure for the detailed study of visual information processing and its disturbance in mental disorders.

Figure Legends

Figure 1 – Visual field Localizer Paradigm

The task consisted of flickering, black-and-white colored checkerboards that appeared randomly at homologous positions of the participant's visual quadrant. Only in 25 % of the trials the two centrally located squares changed their color into yellow for 133 ms. Participants were required to press a response box button when noticing that. During the whole task participants were instructed to fixate a black, x-shaped fixation cross presented in the center of the screen. Checkerboards appeared for 2000 ms. The regular inter-stimulus interval (Shaffer et al.) was 0 ms. Every 10 to 14 trial the ITI extended to 2000 ms.

Figure 2 – Group analysis of visual quadrants

Surface-based group results (a) before and (b) after CBA and averaged time courses. After CBA, group ROIs showed greater spatial consistency and ROIs for the lower visual hemifield were larger in size than ROIs for the upper visual hemifield. Average timecourses (incl. SEM) showed clear position selectivity which was higher after CBA.
ROI/graph colors: red = upper left (UL) visual quadrant, orange = lower left (LL) visual quadrant, light-blue = lower right (LR) visual quadrant, dark-blue = upper right (UR) visual quadrant.

Figure 3 – Probability Maps

Probability Maps (a) before and (b) after CBA for each visual quadrant. The color code grey-to-white indicates an increase in the probability of overlap. Probability maps (a) before CBA showed a maximum probability of overlap of up to 50 %. Probability maps (b) after CBA showed a maximum probability of overlap of up to 90 %.

554 **Figure 4 – Probability Difference Maps**

555 Probability difference maps (post-CBA minus pre-CBA). The color code dark-red-to-white
556 indicates an increase of activation overlap. The color code blue-to-green indicate a decrease
557 of activation overlap. Overall, at the center of each ROI the probability of overlap increased
558 by up to forty percent after CBA.

559

560 **Figure 5 – Average timecourses of visual quadrants**

561 Average timecourses (incl. SEM) of visual quadrants for full single-subject and single-subject
562 extended peak vertex ROIs before and after CBA. Extended peak-vertex ROIs showed
563 consistently larger BOLD-signal amplitudes. Average timecourses showed clear position
564 selectivity which was unaffected by CBA.
565 ROI/graph colors: red = upper left (UL) visual quadrant, orange = lower left (LL) visual
566 quadrant, light-blue = lower right (LR) visual quadrant, dark-blue = upper right (UR) visual
567 quadrant. Dashed lines = single subject extended peak-vertex ROIs, solid lines = full single-
568 subject ROIs.

569

570 **Figure 6 – Peak vertex distribution maps**

571 For each visual quadrant single-subject peak vertices were mapped (a) before and (b) after
572 CBA and a vertex-wise number of peak vertices were computed to estimate the degree of
573 overlap. The color code turquoise-to-red indicates an increase in the degree of overlap. After
574 CBA, we observed reduced spatial variability of peak vertex location.

575

576 **Table 1 – Talairach coordinates**

577 Table 1 depicts the Talairach coordinates of the group ROIs of the corresponding visual
578 quadrants before and after CBA.

579

580

581

582 **Author contributions**

583 All authors made substantial contributions to the conception or design of the work, or the
584 acquisition, analysis, or interpretation of data. AR and RAB acquired funding. RAB, BP, MS
585 and LR designed the experiment. MQ, CVB-S, LR and RAB acquired the data. ER and RG
586 provided analytical tools. MQ and RAB analysed the data. MQ and RAB undertook the
587 literature searches and wrote the first draft of the manuscript. All authors contributed to and
588 revised the manuscript. All authors read and approved the final manuscript.

589

590 **DISCLOSURES**

591 The authors have declared that there are no conflicts of interest in relation to the subject of
592 this study.

593

594 **DATA AVAILABILITY STATEMENT**

595 The data that support the findings of this study are available from the corresponding author
596 upon reasonable request.

597

REFERENCES

Amedi, A., Stern, W. M., Camprodon, J. A., Bermpohl, F., Merabet, L., Rotman, S., . . . Pascual-Leone, A. (2007). Shape conveyed by visual-to-auditory sensory substitution activates the lateral occipital complex. *Nat Neurosci, 10*(6), 687-689. doi:10.1038/nn1912

Anderson, J., Cameron, E., & Levine, M. (2014). A method for quantifying visual field inhomogeneities. *Vision Research, 105*. doi:10.1016/j.visres.2014.09.010

Anticevic, A., Dierker, D. L., Gillespie, S. K., Repovs, G., Csernansky, J. G., Van Essen, D. C., & Barch, D. M. (2008). Comparing surface-based and volume-based analyses of functional neuroimaging data in patients with schizophrenia. *Neuroimage, 41*(3), 835-848. doi:10.1016/j.neuroimage.2008.02.052

Bakroon, A., & Lakshminarayanan, V. (2016). Visual function in autism spectrum disorders: a critical review. *Clin Exp Optom, 99*(4), 297-308. doi:10.1111/cxo.12383

Bedny, M., Pascual-Leone, A., Dodell-Feder, D., Fedorenko, E., & Saxe, R. (2011). Language processing in the occipital cortex of congenitally blind adults. *Proceedings of the National Academy of Sciences, 108*, 4429 - 4434.

Bergmann, J., Genç, E., Kohler, A., Singer, W., & Pearson, J. (2014). Neural Anatomy of Primary Visual Cortex Limits Visual Working Memory. *Cerebral Cortex, 26*(1), 43-50. doi:10.1093/cercor/bhu168

Bittner, R. A., Linden, D. E., Roebroeck, A., Härtling, F., Rotarska-Jagiela, A., Maurer, K., . . . Haenschel, C. (2015). The When and Where of Working Memory Dysfunction in Early-Onset Schizophrenia-A Functional Magnetic Resonance Imaging Study. *Cereb Cortex, 25*(9), 2494-2506. doi:10.1093/cercor/bhu050

Bittner, R. A., Seitz, A., Hahn, P., Raspor, E., Novak, C., Linden, D., . . . Reif, A. (2017). FV 2 Reduced spatial variability in cortical working memory networks after macro-anatomical alignment – Converging evidence from multiple fMRI studies. *Clinical Neurophysiology, 128*(10), e306. doi:https://doi.org/10.1016/j.clinph.2017.06.044

Bressler, D. W., & Silver, M. A. (2010). Spatial attention improves reliability of fMRI retinotopic mapping signals in occipital and parietal cortex. *Neuroimage, 53*(2), 526-533. doi:10.1016/j.neuroimage.2010.06.063

Brett, M., Johnsrude, I. S., & Owen, A. M. (2002). The problem of functional localization in the human brain. *Nat Rev Neurosci, 3*(3), 243-249. doi:10.1038/nrn756

Bridge, H. (2011). Mapping the visual brain: how and why. *Eye (Lond), 25*(3), 291-296. doi:10.1038/eye.2010.166

Brodoehl, S., Gaser, C., Dahnke, R., Witte, O. W., & Klingner, C. M. (2020). Surface-based analysis increases the specificity of cortical activation patterns and connectivity results. *Scientific Reports, 10*(1), 5737. doi:10.1038/s41598-020-62832-z

Bullmore, E., & Sporns, O. (2009). Complex brain networks: graph theoretical analysis of structural and functional systems. *Nature Reviews Neuroscience, 10*(3), 186-198. doi:10.1038/nrn2575

Butler, P. D., Schechter, I., Zemon, V., Schwartz, S. G., Greenstein, V. C., Gordon, J., . . . Javitt, D. C. (2001). Dysfunction of early-stage visual processing in schizophrenia. *Am J Psychiatry, 158*(7), 1126-1133. doi:10.1176/appi.ajp.158.7.1126

Butler, P. D., Silverstein, S. M., & Dakin, S. C. (2008). Visual perception and its impairment in schizophrenia. *Biol Psychiatry, 64*(1), 40-47. doi:10.1016/j.biopsych.2008.03.023

Butler, P. D., Thompson, J. L., Seitz, A. R., Deveau, J., & Silverstein, S. M. (2017). Visual perceptual remediation for individuals with schizophrenia: Rationale, method, and three case studies. *Psychiatr Rehabil J, 40*(1), 43-52. doi:10.1037/prj0000212

Chen, C. Y., Chen, C. L., Wu, C. Y., Chen, H. C., Tang, F. T., & Wong, M. K. (2002). Visual spatial attention in children with attention deficit hyperactivity disorder. *Chang Gung Med J, 25*(8), 514-521.

Chen, H., Yao, D., & Liu, Z. (2004). A study on asymmetry of spatial visual field by analysis of the fMRI BOLD response. *Brain Topogr, 17*(1), 39-46. doi:10.1023/b:brat.0000047335.00110.6a

650 Conroy, B. R., Singer, B. D., Guntupalli, J. S., Ramadge, P. J., & Haxby, J. V. (2013). Inter-subject
651 alignment of human cortical anatomy using functional connectivity. *Neuroimage, 81*, 400-
652 411. doi:https://doi.org/10.1016/j.neuroimage.2013.05.009
653 Corbetta, M., & Shulman, G. L. (2002). Control of goal-directed and stimulus-driven attention in the
654 brain. *Nature Reviews Neuroscience, 3*(3), 201-215. doi:10.1038/nrn755
655 Curcio, C. A., & Allen, K. A. (1990). Topography of ganglion cells in human retina. *J Comp Neurol,*
656 *300*(1), 5-25. doi:10.1002/cne.903000103
657 Cuthbert, B. N. (2014). The RDoC framework: facilitating transition from ICD/DSM to dimensional
658 approaches that integrate neuroscience and psychopathology. *World Psychiatry, 13*(1), 28-
659 35. doi:10.1002/wps.20087
660 Das, M., Bennett, D. M., & Dutton, G. N. (2007). Visual attention as an important visual function: an
661 outline of manifestations, diagnosis and management of impaired visual attention. *Br J*
662 *Ophthalmol, 91*(11), 1556-1560. doi:10.1136/bjo.2006.104844
663 de Haan, B., Bither, M., Brauer, A., & Karnath, H. O. (2015). Neural Correlates of Spatial Attention and
664 Target Detection in a Multi-Target Environment. *Cereb Cortex, 25*(8), 2321-2331.
665 doi:10.1093/cercor/bhu046
666 Desai, R., Liebenthal, E., Possing, E. T., Waldron, E., & Binder, J. R. (2005). Volumetric vs. surface-
667 based alignment for localization of auditory cortex activation. *Neuroimage, 26*(4), 1019-1029.
668 doi:10.1016/j.neuroimage.2005.03.024
669 Di Russo, F., Martínez, A., & Hillyard, S. A. (2003). Source analysis of event-related cortical activity
670 during visuo-spatial attention. *Cereb Cortex, 13*(5), 486-499. doi:10.1093/cercor/13.5.486
671 Di Russo, F., Martínez, A., Sereno, M. I., Pitzalis, S., & Hillyard, S. A. (2002). Cortical sources of the
672 early components of the visual evoked potential. *Hum Brain Mapp, 15*(2), 95-111.
673 doi:10.1002/hbm.10010
674 Dougherty, R. F., Koch, V. M., Brewer, A. A., Fischer, B., Modersitzki, J., & Wandell, B. A. (2003). Visual
675 field representations and locations of visual areas V1/2/3 in human visual cortex. *J Vis, 3*(10),
676 586-598. doi:10.1167/3.10.1
677 Downing, P. E., Chan, A. W., Peelen, M. V., Dodds, C. M., & Kanwisher, N. (2006). Domain specificity
678 in visual cortex. *Cereb Cortex, 16*(10), 1453-1461. doi:10.1093/cercor/bhj086
679 Dumoulin, S. O., & Wandell, B. A. (2008). Population receptive field estimates in human visual cortex.
680 *Neuroimage, 39*(2), 647-660. doi:10.1016/j.neuroimage.2007.09.034
681 Eickhoff, S. B., Rottschy, C., Kujovic, M., Palomero-Gallagher, N., & Zilles, K. (2008). Organizational
682 Principles of Human Visual Cortex Revealed by Receptor Mapping. *Cerebral Cortex, 18*(11),
683 2637-2645. doi:10.1093/cercor/bhn024
684 Evans, A. C., Collins, D., Mills, S. R., Brown, E., Kelly, R., & Peters, T. (1993). 3D statistical
685 neuroanatomical models from 305 MRI volumes. *1993 IEEE Conference Record Nuclear*
686 *Science Symposium and Medical Imaging Conference*, 1813-1817 vol.1813.
687 Fedorenko, E., Hsieh, P. J., Nieto-Castañón, A., Whitfield-Gabrieli, S., & Kanwisher, N. (2010). New
688 method for fMRI investigations of language: defining ROIs functionally in individual subjects.
689 *J Neurophysiol, 104*(2), 1177-1194. doi:10.1152/jn.00032.2010
690 Fischl, B., Sereno, M. I., & Dale, A. M. (1999). Cortical surface-based analysis. II: Inflation, flattening,
691 and a surface-based coordinate system. *Neuroimage, 9*(2), 195-207.
692 doi:10.1006/nimg.1998.0396
693 Fischl, B., Sereno, M. I., Tootell, R. B., & Dale, A. M. (1999). High-resolution intersubject averaging
694 and a coordinate system for the cortical surface. *Hum Brain Mapp, 8*(4), 272-284.
695 doi:10.1002/(sici)1097-0193(1999)8:4<272::aid-hbm10>3.0.co;2-4
696 French, L., & Paus, T. (2015). A FreeSurfer view of the cortical transcriptome generated from the
697 Allen Human Brain Atlas. *Frontiers in Neuroscience, 9*(323). doi:10.3389/fnins.2015.00323
698 Frost, & Goebel. (2012). Measuring structural-functional correspondence: spatial variability of
699 specialised brain regions after macro-anatomical alignment. *Neuroimage, 59*(2), 1369-1381.
700 doi:10.1016/j.neuroimage.2011.08.035

Frost, & Goebel. (2013). Functionally informed cortex based alignment: an integrated approach for whole-cortex macro-anatomical and ROI-based functional alignment. *Neuroimage, 83*, 1002-1010. doi:10.1016/j.neuroimage.2013.07.056

Glasser, M. F., Coalson, T. S., Robinson, E. C., Hacker, C. D., Harwell, J., Yacoub, E., . . . Van Essen, D. C. (2016). A multi-modal parcellation of human cerebral cortex. *Nature, 536*(7615), 171-178. doi:10.1038/nature18933

Goebel, R., Esposito, F., & Formisano, E. (2006). Analysis of functional image analysis contest (FIAC) data with brainvoyager QX: From single-subject to cortically aligned group general linear model analysis and self-organizing group independent component analysis. *Hum Brain Mapp, 27*(5), 392-401. doi:10.1002/hbm.20249

Goodale, M., & Milner, D. (2006). One brain - Two visual systems. *Psychologist, 19*, 660-663.

Greve, D. N., & Fischl, B. (2009). Accurate and robust brain image alignment using boundary-based registration. *Neuroimage, 48*(1), 63-72. doi:10.1016/j.neuroimage.2009.06.060

Gulban, O. F., Goebel, R., Moerel, M., Zachlod, D., Mohlberg, H., Amunts, K., & de Martino, F. (2020). Improving a probabilistic cytoarchitectonic atlas of auditory cortex using a novel method for inter-individual alignment. *Elife, 9*, e56963. doi:10.7554/eLife.56963

Haenschel, C., Bittner, R. A., Haertling, F., Rotarska-Jagiela, A., Maurer, K., Singer, W., & Linden, D. E. (2007). Contribution of impaired early-stage visual processing to working memory dysfunction in adolescents with schizophrenia: a study with event-related potentials and functional magnetic resonance imaging. *Arch Gen Psychiatry, 64*(11), 1229-1240. doi:10.1001/archpsyc.64.11.1229

Hagler, D. J., Jr. (2014). Visual field asymmetries in visual evoked responses. *J Vis, 14*(14), 13. doi:10.1167/14.14.13

Hahn, B., Shrieves, M. E., Olmstead, C. K., Yuille, M. B., Chiappelli, J. J., Pereira, E. F. R., . . . Fawcett, W. P. (2020). Evidence for positive allosteric modulation of cognitive-enhancing effects of nicotine in healthy human subjects. *Psychopharmacology, 237*(1), 219-230. doi:10.1007/s00213-019-05363-4

Hale, T. S., Kane, A. M., Kaminsky, O., Tung, K. L., Wiley, J. F., McGough, J. J., . . . Kaplan, J. T. (2014). Visual Network Asymmetry and Default Mode Network Function in ADHD: An fMRI Study. *Front Psychiatry, 5*, 81. doi:10.3389/fpsyt.2014.00081

Harrison, S. A., & Tong, F. (2009). Decoding reveals the contents of visual working memory in early visual areas. *Nature, 458*(7238), 632-635. doi:10.1038/nature07832

Hawrylycz, M. J., Lein, E. S., Guillozet-Bongaarts, A. L., Shen, E. H., Ng, L., Miller, J. A., . . . Jones, A. R. (2012). An anatomically comprehensive atlas of the adult human brain transcriptome. *Nature, 489*(7416), 391-399. doi:10.1038/nature11405

Hinds, O. P., Rajendran, N., Polimeni, J. R., Augustinack, J. C., Wiggins, G., Wald, L. L., . . . Fischl, B. (2008). Accurate prediction of V1 location from cortical folds in a surface coordinate system. *Neuroimage, 39*(4), 1585-1599. doi:10.1016/j.neuroimage.2007.10.033

Huang, T., Chen, X., Jiang, J., Zhen, Z., & Liu, J. (2019). A probabilistic atlas of the human motion complex built from large-scale functional localizer data. *Hum Brain Mapp, 40*(12), 3475-3487. doi:10.1002/hbm.24610

Insel, T. R. (2014). The NIMH Research Domain Criteria (RDoC) Project: precision medicine for psychiatry. *Am J Psychiatry, 171*(4), 395-397. doi:10.1176/appi.ajp.2014.14020138

Julian, J. B., Fedorenko, E., Webster, J., & Kanwisher, N. (2012). An algorithmic method for functionally defining regions of interest in the ventral visual pathway. *Neuroimage, 60*(4), 2357-2364. doi:10.1016/j.neuroimage.2012.02.055

Kanwisher, N., McDermott, J., & Chun, M. M. (1997). The fusiform face area: a module in human extrastriate cortex specialized for face perception. *J Neurosci, 17*(11), 4302-4311. doi:10.1523/jneurosci.17-11-04302.1997

Kraft, A., Schira, M. M., Hagendorf, H., Schmidt, S., Olma, M., & Brandt, S. A. (2005). fMRI localizer technique: efficient acquisition and functional properties of single retinotopic positions in the human visual cortex. *Neuroimage, 28*(2), 453-463. doi:10.1016/j.neuroimage.2005.05.050

753 Kriegeskorte, N., & Goebel, R. (2001). An Efficient Algorithm for Topologically Correct Segmentation
754 of the Cortical Sheet in Anatomical MR Volumes. *Neuroimage, 14*, 329-346.
755 Lee, J., Reavis, E. A., Engel, S. A., Altshuler, L. L., Cohen, M. S., Glahn, D. C., . . . Green, M. F. (2019).
756 fMRI evidence of aberrant neural adaptation for objects in schizophrenia and bipolar
757 disorder. *Hum Brain Mapp, 40*(5), 1608-1617. doi:10.1002/hbm.24472
758 Liu, T., Heeger, D. J., & Carrasco, M. (2006). Neural correlates of the visual vertical meridian
759 asymmetry. *J Vis, 6*(11), 1294-1306. doi:10.1167/6.11.12
760 Loughnane, G. M., Shanley, J. P., Lalor, E. C., & O'Connell, R. G. (2015). Behavioral and
761 electrophysiological evidence of opposing lateral visuospatial asymmetries in the upper and
762 lower visual fields. *Cortex, 63*, 220-231. doi:10.1016/j.cortex.2014.09.003
763 Manoach, D. S. (2003). Prefrontal cortex dysfunction during working memory performance in
764 schizophrenia: reconciling discrepant findings. *Schizophr Res, 60*(2-3), 285-298.
765 doi:10.1016/s0920-9964(02)00294-3
766 Nieto-Castañón, A., & Fedorenko, E. (2012). Subject-specific functional localizers increase sensitivity
767 and functional resolution of multi-subject analyses. *Neuroimage, 63*(3), 1646-1669.
768 doi:10.1016/j.neuroimage.2012.06.065
769 Norman, L., & Thaler, L. (2019). Retinotopic-like maps of spatial sound in primary visuaå cortex of
770 blind human echolocators. *Proceedings of the Royal Society B: Biological Sciences, 286*.
771 O'Connell, C., Ho, L. C., Murphy, M. C., Conner, I. P., Wollstein, G., Cham, R., & Chan, K. C. (2016).
772 Structural and functional correlates of visual field asymmetry in the human brain by diffusion
773 kurtosis MRI and functional MRI. *Neuroreport, 27*(16), 1225-1231.
774 doi:10.1097/wnr.0000000000000682
775 Oldfield, R. C. (1971). The assessment and analysis of handedness: the Edinburgh inventory.
776 *Neuropsychologia, 9*(1), 97-113. doi:10.1016/0028-3932(71)90067-4
777 Pantazis, D., Joshi, A., Jiang, J., Shattuck, D. W., Bernstein, L. E., Damasio, H., & Leahy, R. M. (2010).
778 Comparison of landmark-based and automatic methods for cortical surface registration.
779 *Neuroimage, 49*(3), 2479-2493. doi:10.1016/j.neuroimage.2009.09.027
780 Peters, B., Kaiser, J., Rahm, B., & Bledowski, C. (2015). Activity in Human Visual and Parietal Cortex
781 Reveals Object-Based Attention in Working Memory. *The Journal of Neuroscience, 35*(8),
782 3360-3369. doi:10.1523/jneurosci.3795-14.2015
783 Ptito, M., Matteau, I., Gjedde, A., & Kupers, R. (2009). Recruitment of the middle temporal area by
784 tactile motion in congenital blindness. *Neuroreport, 20*(6), 543-547.
785 doi:10.1097/WNR.0b013e3283279909
786 Reich, L., Szwed, M., Cohen, L., & Amedi, A. (2011). A ventral visual stream reading center
787 independent of visual experience. *Curr Biol, 21*(5), 363-368. doi:10.1016/j.cub.2011.01.040
788 Renier, L., Collignon, O., Poirier, C., Tranduy, D., Vanlierde, A., Bol, A., . . . De Volder, A. G. (2005).
789 Cross-modal activation of visual cortex during depth perception using auditory substitution
790 of vision. *Neuroimage, 26*(2), 573-580. doi:10.1016/j.neuroimage.2005.01.047
791 Rosenke, M., van Hoof, R., van den Hurk, J., Grill-Spector, K., & Goebel, R. (2020). A Probabilistic
792 Functional Atlas of Human Occipito-Temporal Visual Cortex. *Cerebral Cortex*.
793 doi:10.1093/cercor/bhaa246
794 Rubin, N., Nakayama, K., & Shapley, R. (1996). Enhanced perception of illusory contours in the lower
795 versus upper visual hemifields. *Science, 271*(5249), 651-653.
796 doi:10.1126/science.271.5249.651
797 Sabuncu, M. R., Singer, B. D., Conroy, B., Bryan, R. E., Ramadge, P. J., & Haxby, J. V. (2009). Function-
798 based Intersubject Alignment of Human Cortical Anatomy. *Cerebral Cortex, 20*(1), 130-140.
799 doi:10.1093/cercor/bhp085
800 Sanz-Cervera, P., Pastor-Cerezuela, G., González-Sala, F., Tárraga-Mínguez, R., & Fernández-Andrés,
801 M.-I. (2017). Sensory Processing in Children with Autism Spectrum Disorder and/or Attention
802 Deficit Hyperactivity Disorder in the Home and Classroom Contexts. *Frontiers in psychology,*
803 *8*, 1772-1772. doi:10.3389/fpsyg.2017.01772

804 Schmidtmann, G., Logan, A. J., Kennedy, G. J., Gordon, G. E., & Loffler, G. (2015). Distinct lower visual
805 field preference for object shape. *J Vis, 15*(5), 18. doi:10.1167/15.5.18
806 Sereno, M. I., Dale, A. M., Reppas, J. B., Kwong, K. K., Belliveau, J. W., Brady, T. J., . . . Tootell, R. B.
807 (1995). Borders of multiple visual areas in humans revealed by functional magnetic
808 resonance imaging. *Science (New York, N.Y.), 268*(5212), 889-893.
809 doi:10.1126/science.7754376
810 Seymour, R. A., Rippon, G., Gooding-Williams, G., Schoffelen, J. M., & Kessler, K. (2019). Dysregulated
811 oscillatory connectivity in the visual system in autism spectrum disorder. *Brain, 142*(10),
812 3294-3305. doi:10.1093/brain/awz214
813 Shaffer, C. L., Hurst, R. S., Scialis, R. J., Osgood, S. M., Bryce, D. K., Hoffmann, W. E., . . . Hajós, M.
814 (2013). Positive allosteric modulation of AMPA receptors from efficacy to toxicity: the
815 interspecies exposure-response continuum of the novel potentiator PF-4778574. *J Pharmacol*
816 *Exp Ther, 347*(1), 212-224. doi:10.1124/jpet.113.204735
817 Shigihara, Y., Hoshi, H., & Zeki, S. (2016). Early visual cortical responses produced by checkerboard
818 pattern stimulation. *Neuroimage, 134*. doi:10.1016/j.neuroimage.2016.03.078
819 Shimizu, V. T., Bueno, O. F., & Miranda, M. C. (2014). Sensory processing abilities of children with
820 ADHD. *Braz J Phys Ther, 18*(4), 343-352. doi:10.1590/bjpt-rbf.2014.0043
821 Silson, E. H., Reynolds, R. C., Kravitz, D. J., & Baker, C. I. (2018). Differential Sampling of Visual Space
822 in Ventral and Dorsal Early Visual Cortex. *The Journal of Neuroscience, 38*(9), 2294-2303.
823 doi:10.1523/jneurosci.2717-17.2018
824 Silverstein, S. M., Berten, S., Essex, B., Kovács, I., Susmaras, T., & Little, D. M. (2009). An fMRI
825 examination of visual integration in schizophrenia. *J Integr Neurosci, 8*(2), 175-202.
826 doi:10.1142/s0219635209002113
827 Steinmetz, H., Fürst, G., & Freund, H. J. (1990). Variation of perisylvian and calcarine anatomic
828 landmarks within stereotaxic proportional coordinates. *AJNR Am J Neuroradiol, 11*(6), 1123-
829 1130.
830 Striem-Amit, E., Cohen, L., Dehaene, S., & Amedi, A. (2012). Reading with sounds: sensory
831 substitution selectively activates the visual word form area in the blind. *Neuron, 76*(3), 640-
832 652. doi:10.1016/j.neuron.2012.08.026
833 Talairach, J., & Tournoux, P. (1988). *Co-planar stereotaxic atlas of the human brain: 3-dimensional*
834 *proportional system : an approach to cerebral imaging*. Stuttgart: Thieme.
835 Thomas, N. A., & Elias, L. J. (2011). Upper and lower visual field differences in perceptual
836 asymmetries. *Brain Res, 1387*, 108-115. doi:10.1016/j.brainres.2011.02.063
837 Tomasello, R., Wennekers, T., Garagnani, M., & Pulvermüller, F. (2019). Visual cortex recruitment
838 during language processing in blind individuals is explained by Hebbian learning. *Scientific*
839 *Reports, 9*(1), 3579. doi:10.1038/s41598-019-39864-1
840 Tong, Y., Chen, Q., Nichols, T. E., Rasetti, R., Callicott, J. H., Berman, K. F., . . . Mattay, V. S. (2016).
841 Seeking Optimal Region-Of-Interest (ROI) Single-Value Summary Measures for fMRI Studies
842 in Imaging Genetics. *PLoS One, 11*(3), e0151391. doi:10.1371/journal.pone.0151391
843 Tost, H., Bilek, E., & Meyer-Lindenberg, A. (2012). Brain connectivity in psychiatric imaging genetics.
844 *Neuroimage, 62*(4), 2250-2260. doi:https://doi.org/10.1016/j.neuroimage.2011.11.007
845 Ungerleider, L. G. (1982). *Two cortical visual systems*.
846 Van Essen, D. C., & Drury, H. A. (1997). Structural and functional analyses of human cerebral cortex
847 using a surface-based atlas. *J Neurosci, 17*(18), 7079-7102. doi:10.1523/jneurosci.17-18-
848 07079.1997
849 Van Essen, D. C., Drury, H. A., Dickson, J., Harwell, J., Hanlon, D., & Anderson, C. H. (2001). An
850 integrated software suite for surface-based analyses of cerebral cortex. *J Am Med Inform*
851 *Assoc, 8*(5), 443-459. doi:10.1136/jamia.2001.0080443
852 Wandell, B. A., Dumoulin, S. O., & Brewer, A. A. (2007). Visual field maps in human cortex. *Neuron,*
853 *56*(2), 366-383. doi:10.1016/j.neuron.2007.10.012
854 Wang, L., Mruczek, R. E., Arcaro, M. J., & Kastner, S. (2015). Probabilistic Maps of Visual Topography
855 in Human Cortex. *Cereb Cortex, 25*(10), 3911-3931. doi:10.1093/cercor/bhu277

Weiner, K. S., Barnett, M. A., Witthoft, N., Golarai, G., Stigliani, A., Kay, K. N., . . . Grill-Spector, K. (2018). Defining the most probable location of the parahippocampal place area using cortex-based alignment and cross-validation. *Neuroimage, 170*, 373-384. doi:10.1016/j.neuroimage.2017.04.040

Yamamoto, H., Fukunaga, M., Takahashi, S., Mano, H., Tanaka, C., Umeda, M., & Ejima, Y. (2012). Inconsistency and uncertainty of the human visual area loci following surface-based registration: Probability and Entropy Maps. *Hum Brain Mapp, 33*(1), 121-129. doi:10.1002/hbm.21200

Yenari, M. A., Xu, L., Tang, X. N., Qiao, Y., & Giffard, R. G. (2006). Microglia potentiate damage to blood-brain barrier constituents: improvement by minocycline in vivo and in vitro. *Stroke, 37*(4), 1087-1093. doi:10.1161/01.STR.0000206281.77178.ac

Zilles, K., Schleicher, A., Langemann, C., Amunts, K., Morosan, P., Palomero-Gallagher, N., . . . Roland, P. E. (1997). Quantitative analysis of sulci in the human cerebral cortex: Development, regional heterogeneity, gender difference, asymmetry, intersubject variability and cortical architecture. *Human Brain Mapping, 5*(4), 218-221. doi:https://doi.org/10.1002/(SICI)1097-0193(1997)5:4<218::AID-HBM2>3.0.CO;2-6

Zito, G. A., Cazzoli, D., Müri, R. M., Mosimann, U. P., & Nef, T. (2016). Behavioral Differences in the Upper and Lower Visual Hemifields in Shape and Motion Perception. *Frontiers in behavioral neuroscience, 10*, 128-128. doi:10.3389/fnbeh.2016.00128

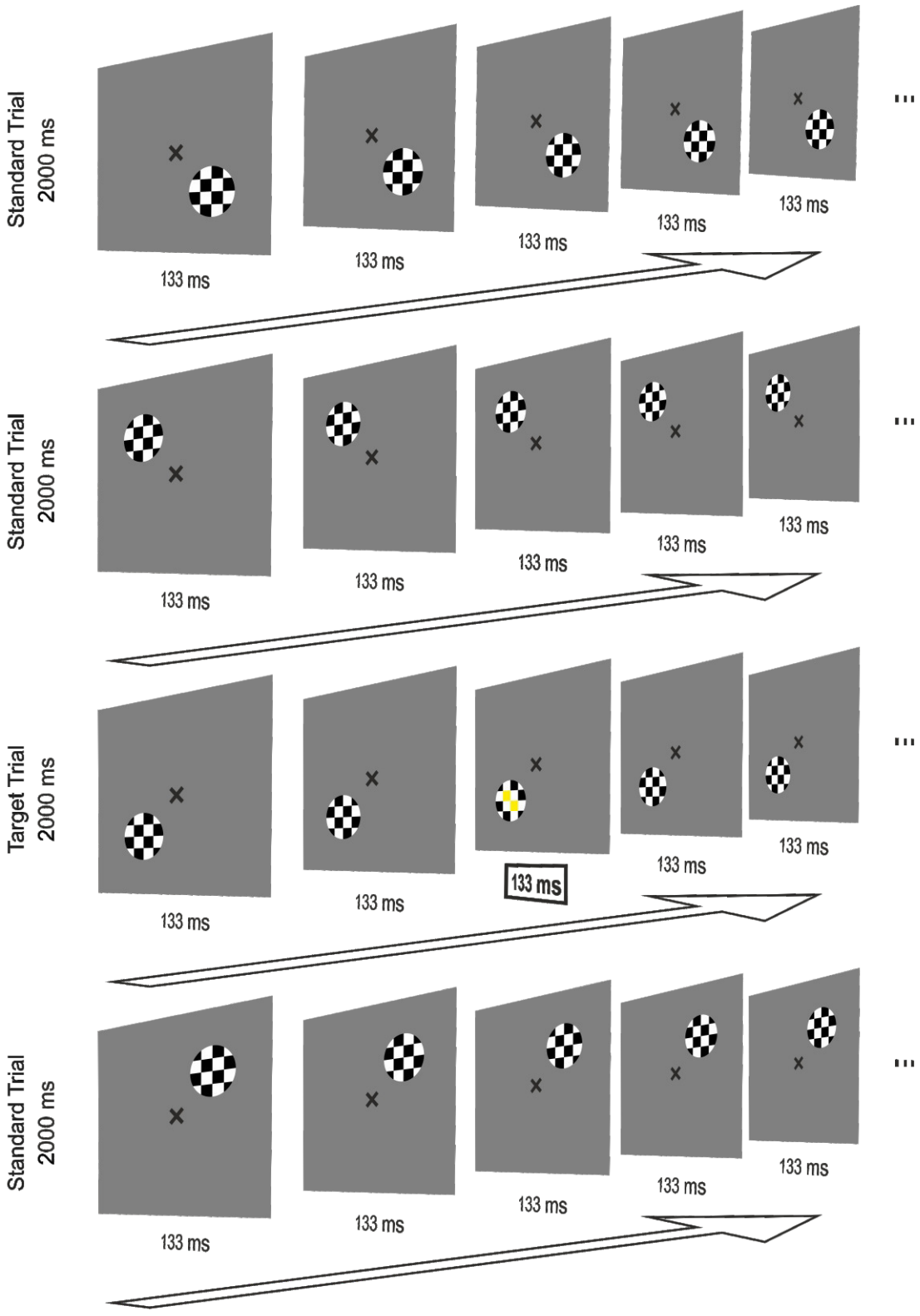

Figure 1

https://doi.org/10.1101/2021.02.26.433066

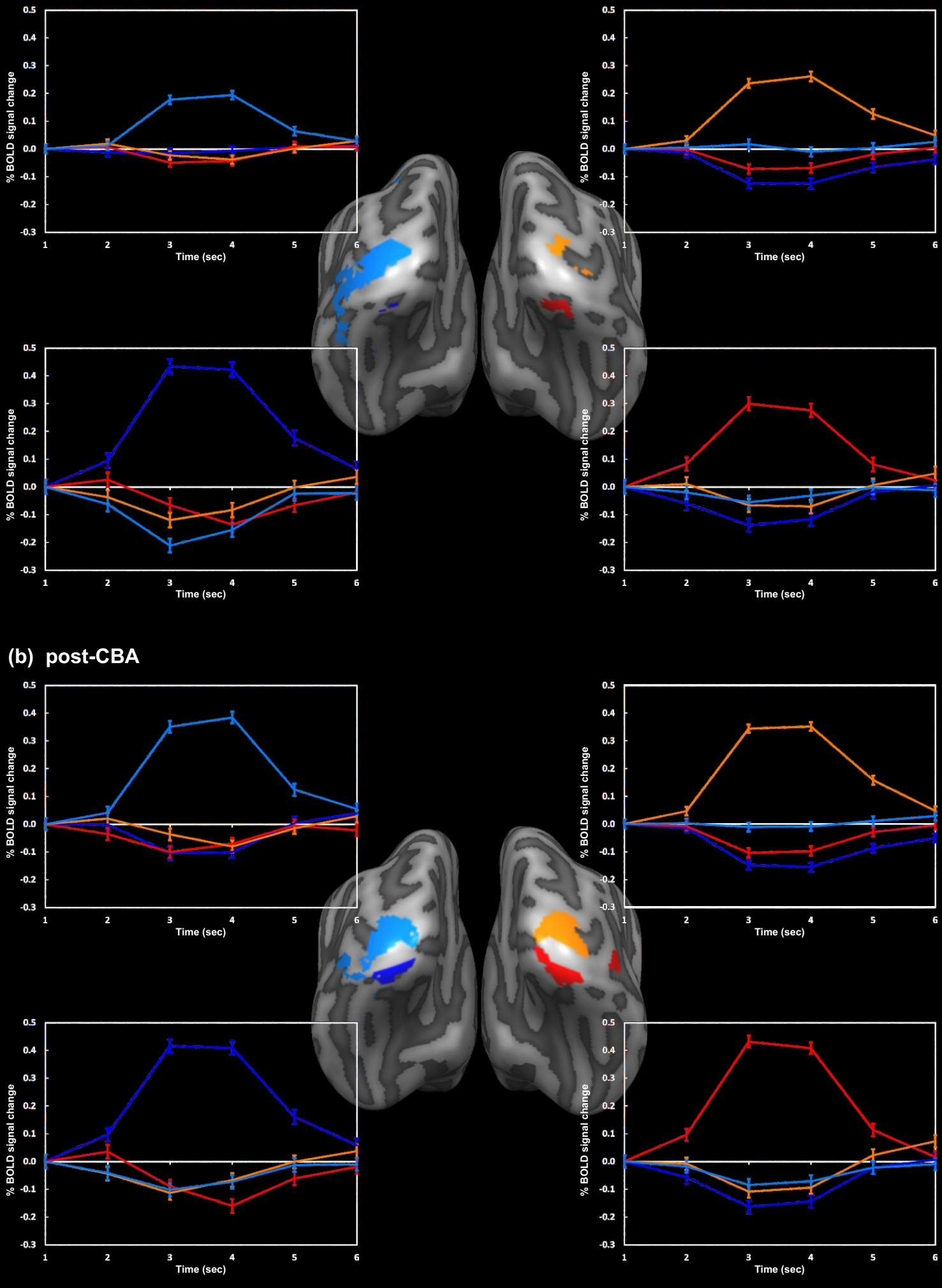

Figure 2

https://doi.org/10.1101/2021.02.26.433066

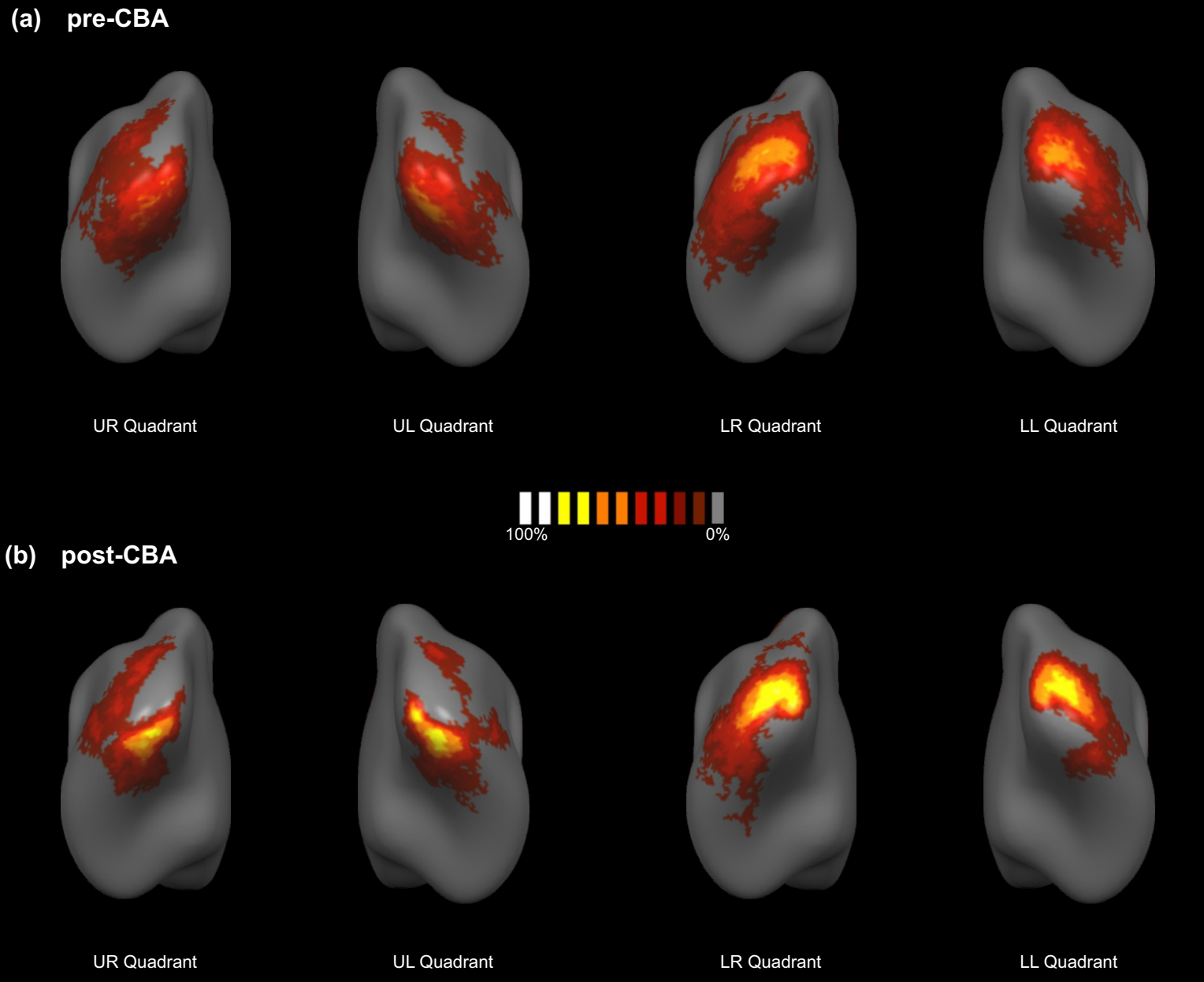

Figure 3

https://doi.org/10.1101/2021.02.26.433066

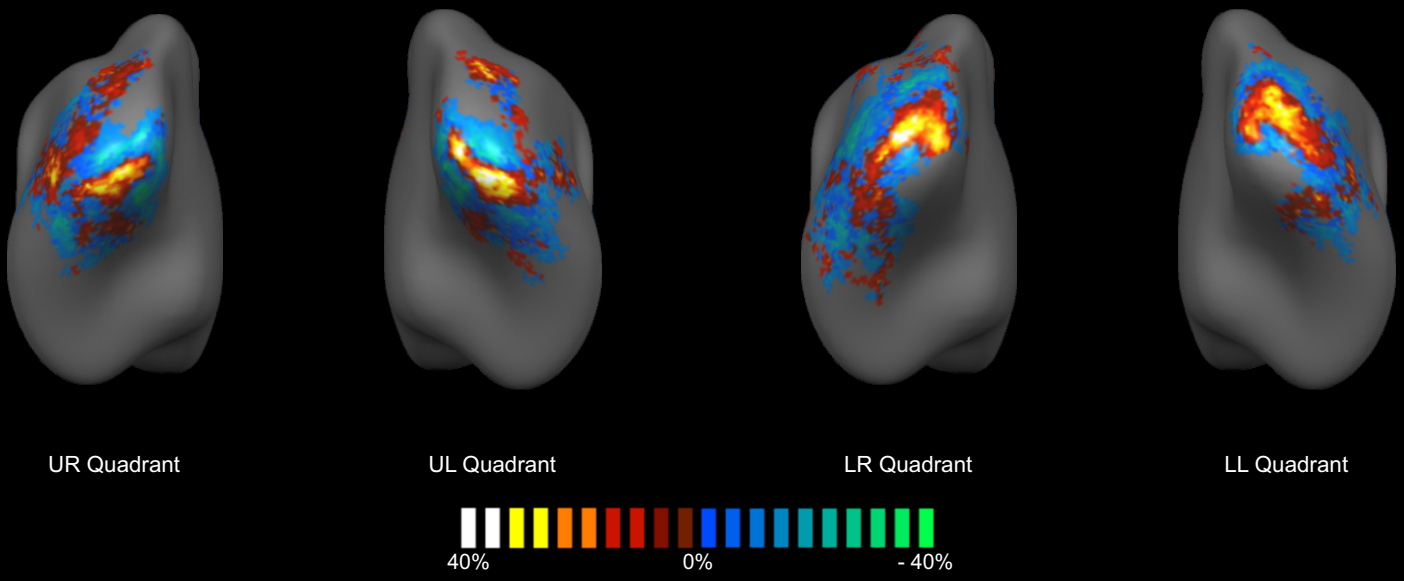

Figure 4

https://doi.org/10.1101/2021.02.26.433066

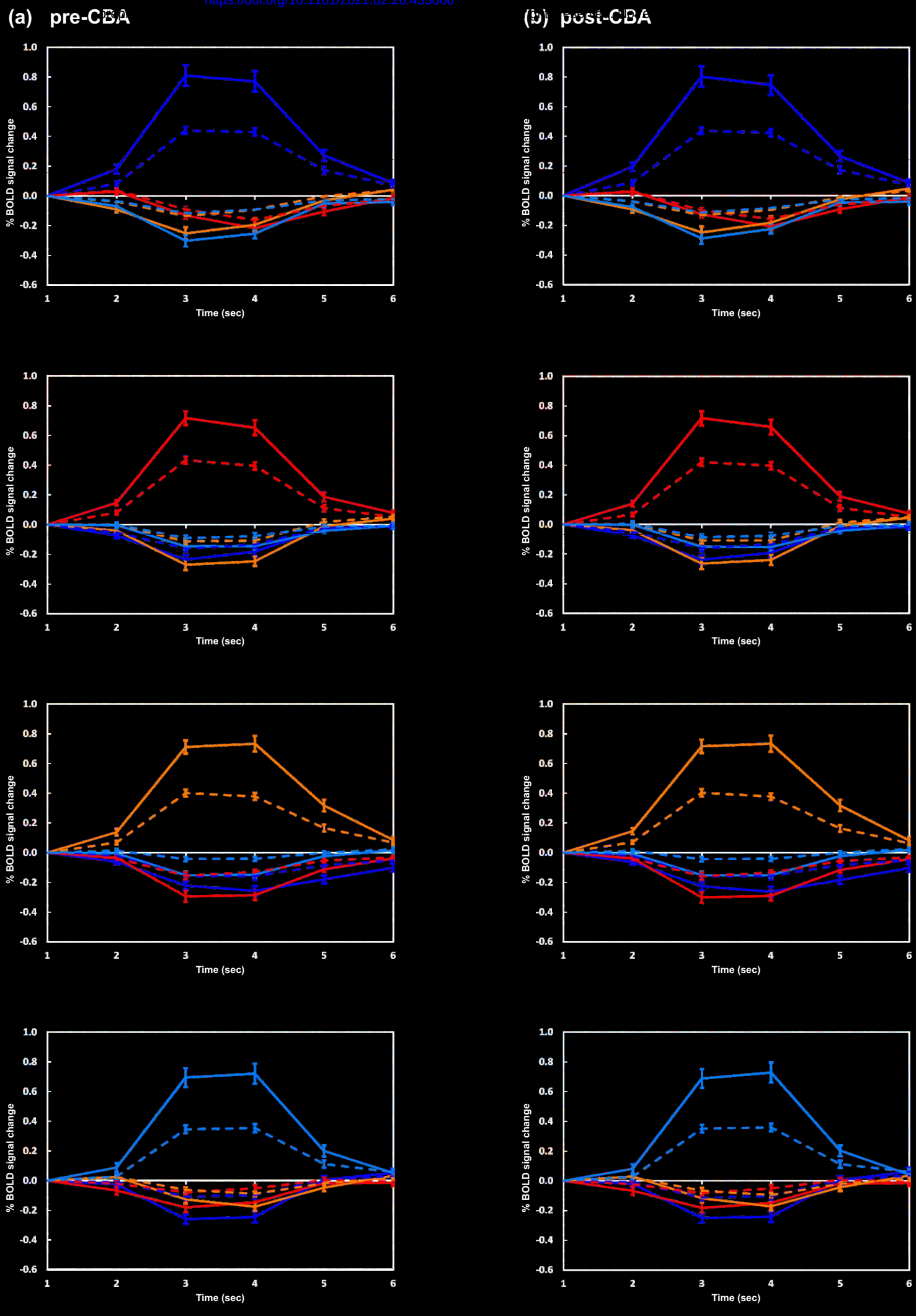

Figure 5

https://doi.org/10.1101/2021.02.26.433066

(a) pre-CBA

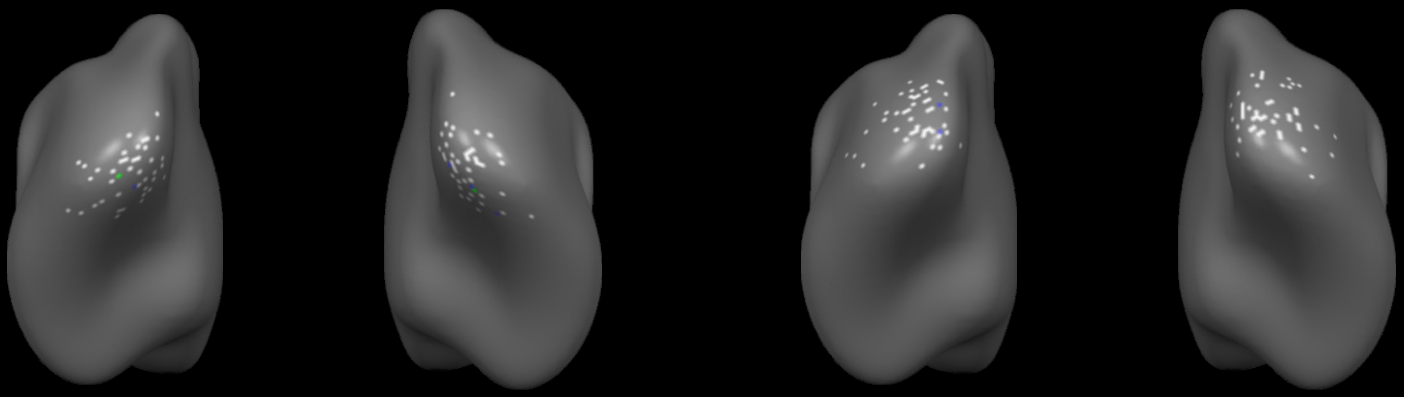

UR Quadrant UL Quadrant LR Quadrant LL Quadrant

(b) post-CBA

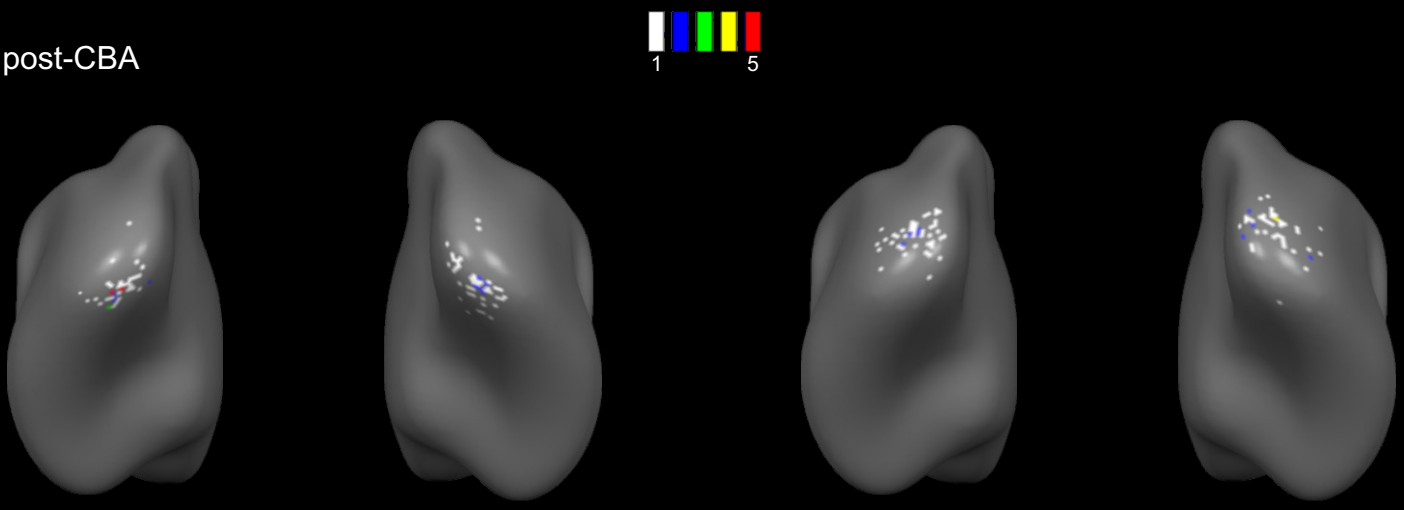

UR Quadrant UL Quadrant LR Quadrant LL Quadrant

Figure 6

Table 1

Region of interest		Number of vertices	Talairach coordinates (in mm)		
			x	y	z
upper right visual quadrant	pre CBA	6	-18	-80	-15
	post CBA	58	-18	-80	-15
upper left visual quadrant	pre CBA	47	24	-75	-14
	post CBA	82	18	-77	-15
lower left visual quadrant	pre CBA	295	-42	-64	5
	post CBA	161	-24	-91	-4
lower right visual quadrant	pre CBA	28	23	-90	3
	post CBA	127	9	-94	-5